

Abbreviations

%N	percentage nitrogen by mass
2-NDPA	2-Nitrodiphenylamine
AIMD	<i>ab initio</i> molecular dynamics
AO	atomic orbital
a.u.	atomic units
B3LYP	Becke, 3-parameter, Lee-Yang-Parr hybrid functional
BCP	bonding critical point
BSSE	basis set superposition error
CH₃CH₃	NC repeat unit with two –OCH ₃ capping groups
CH₃OH	NC repeat unit with –OCH ₃ capping group on ring 1 and –OH group on ring 2
CCP	cage critical point
CP	critical point
DFT	density functional theory
DFT-D	density functional theory with dispersion correction
DSC	differential scanning calorimetry
DOS	degree of substitution
DPA	diphenylamine

EM	energetic materials
EN	ethyl nitrate
ESP	electrostatic potential
G09	Gaussian 09 revision D.01
GGA	generalised gradient approximation
GM	genetically modified
GTO	Gaussian type orbitals
GView	Gauss View 5.0.8
HF	Hartree-Fock
HMF	hydroxymethylfurfural
HOMO	highest occupied molecular orbital
IR	infra-red spectroscopy
KS-DFT	Kohn-Sham DFT
LDA	local density approximation
MD	molecular dynamics
MEP	minimum energy path
MM	molecular mechanics
MMFF94	Merck molecular force field 94
MO	molecular orbitals
MP2	Møller–Plesset perturbation theory with second order correction
MW	molecular weight
NBO	natural bond orbital
NC	nitrocellulose

NCP	nuclear critical point
NG	nitroglycerine
NMR	nuclear magnetic resonance spectroscopy
OHCH₃	NC repeat unit with –OH capping group on ring 1 and –OCH ₃ group on ring 2
PCM	polarisable continuum model
PES	potential energy surface
PETN	pentaerythritol tetranitrate
PETRIN	pentaerythritol trinitrate
QM	quantum mechanics
QTAIM	quantum theory of atoms in molecules
RCP	ring critical point
RESP	restrained electrostatic potential atomic partial charges
RHF	restricted HF
ROHF	restricted-open HF
UHF	unrestricted HF
SB59	1,4-bis(ethylamino)-9,10-anthraquinone dye
SCF	self-consistent field
SEM	scanning electron microscopy
SMD	solvation model based on density
S_N2	bi-molecular nucleophilic substitution reaction
STO	Slater type orbitals
TG	thermogravimetric analysis

TS	transition state
UFF	universal force field
UV	ultraviolet
UV-vis	ultraviolet–visible spectroscopy
vdW	van der Waals
ωB97X-D	ω B97X-D long-range corrected hybrid functional
ZPE	zero-point energy

Chapter 1

Post-Denitration Reactions

1.1 Introduction

Products of the preliminary denitration step of nitrocellulose (NC) can be evolved as gases or remain trapped in the polymer matrix. Reactive nitrogen dioxide radicals generated from homolysis of the O-N bond are likely to migrate within the bulk and attack other sites on the polysaccharide, initiating branched radical chain reactions. These lead to deeper decomposition of the polymer *via* chain scission and rupture of glucose rings, with eventual complete disintegration of the molecule, assisted by products released by ongoing acid hydrolysis. Nitrous and nitric acids are released directly from denitration or via transformation of released NO_x species. In addition to catalysing hydrolysis, they increase the acidity of the overall system, lowering the pH and stimulating further hydrolytic processes [1]. The final product mixture is dictated by the numerous side reactions involving autocatalysis, radical reactions and product interactions.

When studying the ageing of NC using ultraviolet-visible spectroscopy, Moniruzzaman *et al.* observed increasing concentrations of reaction products beyond those generated from first-stage decomposition, following heat treatment over extended timescales [2, 3]. The reaction of the 1,4-bis(ethylamino)-9,10-anthraquinone (1,4-bis(ethylamino)-9,10-anthraquinone dye (SB59)) with NO_x released by denitration, mimics the action of stabilisers such as diphenylamine (DPA) and 2-Nitrodiphenylamine (2-NDPA) commonly used in NC formulations (figure 1.1). The secondary amine groups of the dye consume any nitrates in the system, eliminating the possibility of successive reactions generating acidic species. Un-aged NC thin films, and films aged at 40°C, 50°C, 60°C and 70°C for timescales of up to 2000hrs for 40°C, were compared. UV absorbances at 600 nm and 650 nm were characteristic of the SB59 dye used to indicate the presence of NO_x, released

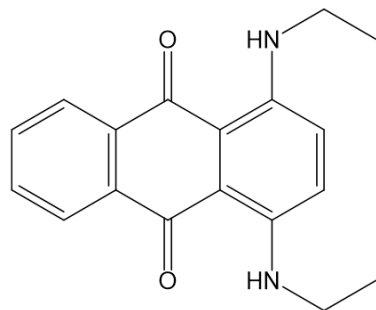


Figure 1.1: 1,4-bis(ethylamino)-9,10-anthraquinone dye (SB59) used to probe the release of nitrates from NC using ultraviolet-visible spectroscopy (UV-vis) and ^1H NMR spectroscopy [3]. The action of nitrate absorption by the dye imitates that of stabilisers commonly used with nitrate ester formulations.

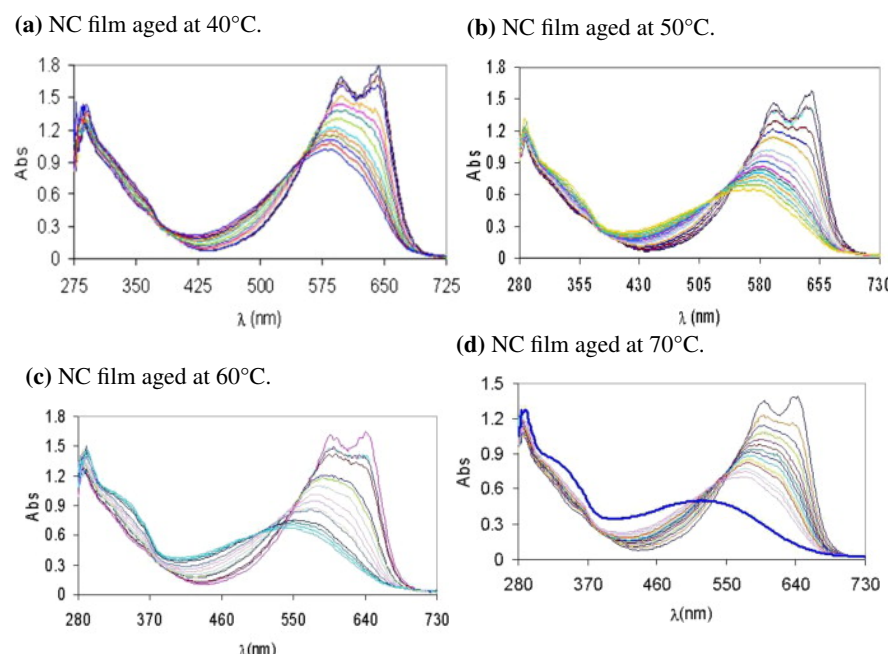


Figure 1.2: UV-vis spectra of aged NC-based film, from the work of Moniruzzaman *et al.*[3]. The peaks at 600 nm and 650 nm are attributed to the $\pi - \pi^*$ transitions in the anthraquinone dye (SB59). Spectral lines with highest absorbance peaks in this region correspond to the sample prior to heat treatment. Peaks below 400 nm indicate the formation of SB59 derivatives due to secondary reactions.

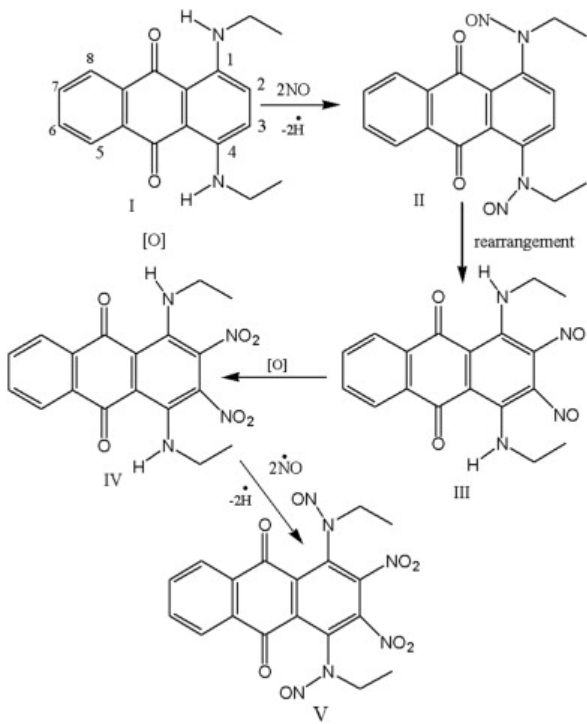
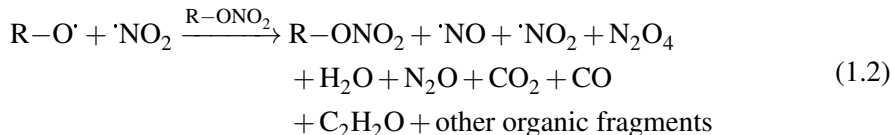
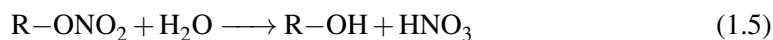


Figure 1.3: Proposed pathway for the reaction of SB59 dye with ·NO released as a result of denitration of NC [3].

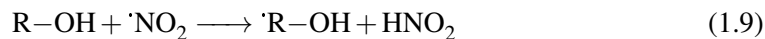
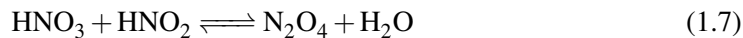
by the denitration of NC (figure 1.2). The isosbestic point identified at 552 nm showed a proportional relationship between the concentration of SB59 as it decreased, with the concentration of the [SB59 + NC] product as it increased. Samples exposed to higher ageing temperatures presented spectra dominated by products formed *via* secondary reactions. For samples aged at temperatures >40°C, the isosbestic point demonstrated a downwards shift with increasing dye consumption. In the case of the 70°C treated run, the final measurement (indicated by the royal-blue line in bold in figure 1.2d)) deviated from the isosbestic point entirely, with more than 81% consumption of the original dye concentration. The drift from the isosbestic point, in addition to the appearance of new absorbance peaks below 400 nm, allude to the presence of new species in the reaction mixture not generated by the primary reaction of SB59 and NC. It is likely that these arise from the continued reaction of SB59 derivatives with NC degradation products, or further derivatives thereof, as suggested in figure 1.3. Following cleavage of the nitrate ester via homolytic fission, elimination of nitrous acid, or hydrolysis, the resulting residues available for further reaction with the polymer or other free molecules in the system. In the study of pentaerythritol tetranitrate (PETN) ageing at high temperatures (115°C - 135°C) in vacuum, and low temperatures (20°C - 65°C) in acetonitrile solution, Sheppard *et al.* commented that thermolysis produced a more com-

Scheme 1.1: Thermolytic initiation

Propagation

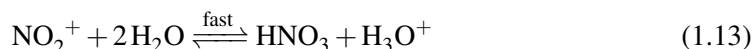
**Scheme 1.2: Hydrolytic initiation**

Propagation



plex and varied mixture, due to deeper degradation and recombination of radicals [4]. By contrast, the low temperature hydrolytic process emphasised formation of pentaerythritol trinitrate (PETRIN) followed by side reactions with reduced likelihood of radical recombination in solution compared to in a solid, as $\cdot\text{NO}_2$ would be more likely to diffuse and react elsewhere. Chin *et al.* proposed schemes for the propagation of secondary reactions initiated by both the thermolysis (scheme 1.1) and hydrolysis of nitrate esters (scheme 1.2) [5].

Termination reactions were not emphasised in either of the schemes for these cases. The hydrolysis scheme was adapted from an earlier work by Camera *et al.* involving the nitrate

Scheme 1.3: Hydrolysis scheme for ethyl nitrate

ester decomposition and subsequent reactions of ethyl nitrate (EN) (where R = CH₃CH₂ for the scheme above) [6]. The original study included an expansion of the hydrolysis step (equation 1.11), where the involvement of NO₂⁺ was illustrated (scheme 1.3).

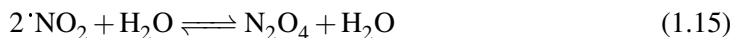
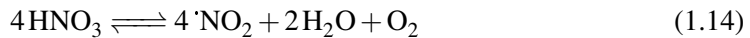
It was highlighted by Camera, that the oxidation of alcohol by nitric acid (equation 1.6) is slow and thus rate-limiting. The mechanism is likely to occur *via* a series of intermediate reactions of which the details are not known. Following the generation of nitrous acid, subsequent oxidations occur rapidly. According to Rigas *et al.*, alcohols are more susceptible to wet oxidation than esters [7]. A higher concentration of unsubstituted hydroxyl groups in the system, and therefore a fewer nitrate ester groups (or a lower degree of substitution (DOS) value), decreases overall stability.

Equations 1.7 - 1.10 describe a possible branched radical chain mechanism, fed by the nitrous and nitric acids produced during the hydrolysis and alcohol oxidation reactions during the initiation stage. By contrast, the propagation reactions in the branched radical chain mechanism for thermolysis are poorly characterised (equation 1.2), defined only by the observable products. This is likely due to their rapid and varied nature, rendering it difficult to follow spectroscopically.

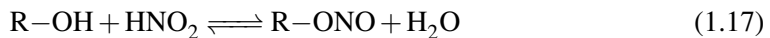
Aellig *et al.* presented an alternative scheme for the decomposition of benzyl nitrate (R = PhCH₂), involving more interaction with the solvent [8]:

Both the Camera/Chin and Aellig schemes above produce final end products observed in

Scheme 1.4: HNO₃ decomposition initiation



Propagation



Termination



the decomposition of NC. In particular, Aellig's scheme accounts for the production of N₂O, which forms a significant part of the decomposition eluent [9]. Whilst the schemes do not propose an exhaustive description of the full spectrum of reactions that take place in the NC matrix during its slow ageing, the early stage reactions of the key species responsible for decomposition are encapsulated.

It is widely agreed that first-stage decomposition follows a first-order process (or pseudo-first order, with respect to hydrolysis reactions). A number of studies observe catalytic rate of decay for the longer-term aging processes. Dauerman [10] observed that when NC was treated with NO₂ gas before heating, the time required for sample ignition halved. He suggested that the NO₂ adsorbed onto the surface acted as a catalysing agent.

Neutral and alkaline hydrolysis reactions follow a pseudo-first order process, however it has been suggested that the presence of acid facilitates a catalytic rate of degradation after an initial incubation period. Multiple studies have addressed the decomposition reactions of nitrate esters following the initial scission of the nitrate group [11, 6, 12, 13, 1] In their work looking into the atmospheric reactions of methylnitrate and methylperoxy nitrate Arenas suggested it was possible for the homolytic denitration reaction of methylnitrate to share a common peroxy intermediate with the peroxide [14]. This could account for some of the lower order NO_x generated. In this section, secondary and extended reaction schemes for the low temperature ageing of NC are explored. Decomposition pathways defined by Chin, Camera and Aellig *et al.* are probed to determine the reactions responsible for the experimentally observed degradation products. The reactions found to be energetically feasible from the proposed routes will be scrutinised to determine whether an autocatalytic pathway can be formed from the thermodynamically validated reaction schemes.

1.2 Methodology

The schemes proposed by Chin, Camera and Aellig *et al.* were used to construct possible degradation routes for NC with the products of homolytic fission, elimination of HNO₂ and acid hydrolysis used as the starting point. Pathways were constructed based on propagation of the given reactions in a step-wise fashion; subsequent reactions were dependent on the products generated in preceding steps. An abundance of water and oxygen were assumed present in the system, attributed to air exposure under the wetted storage conditions of NC. Unsubstituted alcohol moieties (R-OH) were also presumed available, due to incomplete nitration during the synthesis of NC [15], and re-generation following denitration *via* hy-

drolysis. The schemes were modelled with EN, then expanded to the NC monomer. Free energies of reaction (ΔG) were used to determine the feasibility of each reaction.

1.2.1 Computational details

All geometry optimisations were conducted in Gaussian 09 revision D.01 (G09), using the ω B97X-D and B3LYP functionals. Optimisations and thermochemistry calculations were performed to the level of 6-31+G(2df,p) with tight convergence criteria (table ??). Calculations were performed in both vacuum and with polarisable continuum model (PCM) to introduce implicit solvent effects. Chemical species were constructed using Gauss View 5.0.8 (GView) and for molecules of more than 3 atoms, the “Clean” function was used to re-order atoms to a preliminary starting geometry. Energies of optimised structures were checked against values listed on NIST Computational Chemistry Comparison and Benchmark Database [16] if analogous molecules to a similar level of theory were available.

1.3 Results and Discussion

Simplified schemes for the possible ageing reactions of nitrate esters beginning from homolytic fission, elimination of HNO_2 or acid hydrolysis are illustrated in schemes 1.5 - 1.7. When starting with the products of homolytic fission, a branched radical chain mechanism dominates. $\cdot\text{NO}_2$ and HNO_2 were consumed and regenerated, supporting the theory that these may be species contributing to the observed autocatalytic rate of decomposition, following a first-order rate induction period [17, 18, 19]. For all schemes, $\text{R}=\text{O}$ and N_2O were terminating species. Whilst N_2O is released into the environment, $\text{R}=\text{O}$ remains in the system and may go on to participate in further decomposition reactions leading to ring opening. The protonation site of EN was inspected to determine whether it matched that of the hydrolytic denitration of NC, therefore following the same extended hydrolysis scheme.

Table 1.1: Free energies of protonation for each oxygen site on EN.

Protonated site		$\Delta G_r / \text{kcal mol}^{-1}$			
		ω B97X-D	PCM	B3LYP	PCM
Terminal (upper)	$\text{CH}_3\text{CH}_3\text{ONO}_2\text{H}^+$	-12.28	8.82	-13.78	5.63
Terminal (lower)	$\text{CH}_3\text{CH}_3\text{ONO}_2\text{H}^+$	-9.48	9.46	-11.13	5.65
Bridging	$\text{CH}_3\text{CH}_3\text{O}(\text{H}^+)\text{NO}_2$	-9.32	9.06	-15.31	6.67

Table 1.1 shows the protonation energies for the three different oxygen sites on EN. Despite the upper terminal oxygen possessing the most thermodynamically favourable en-

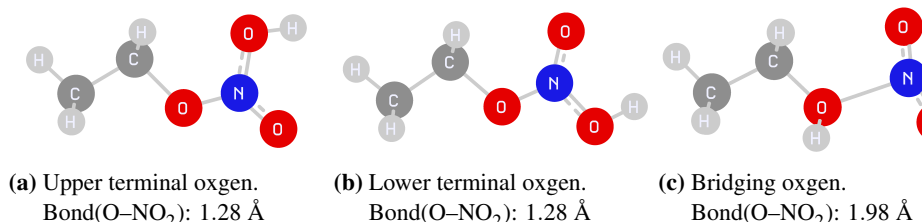


Figure 1.4: Optimised geometries of the possible protonation sites on EN.

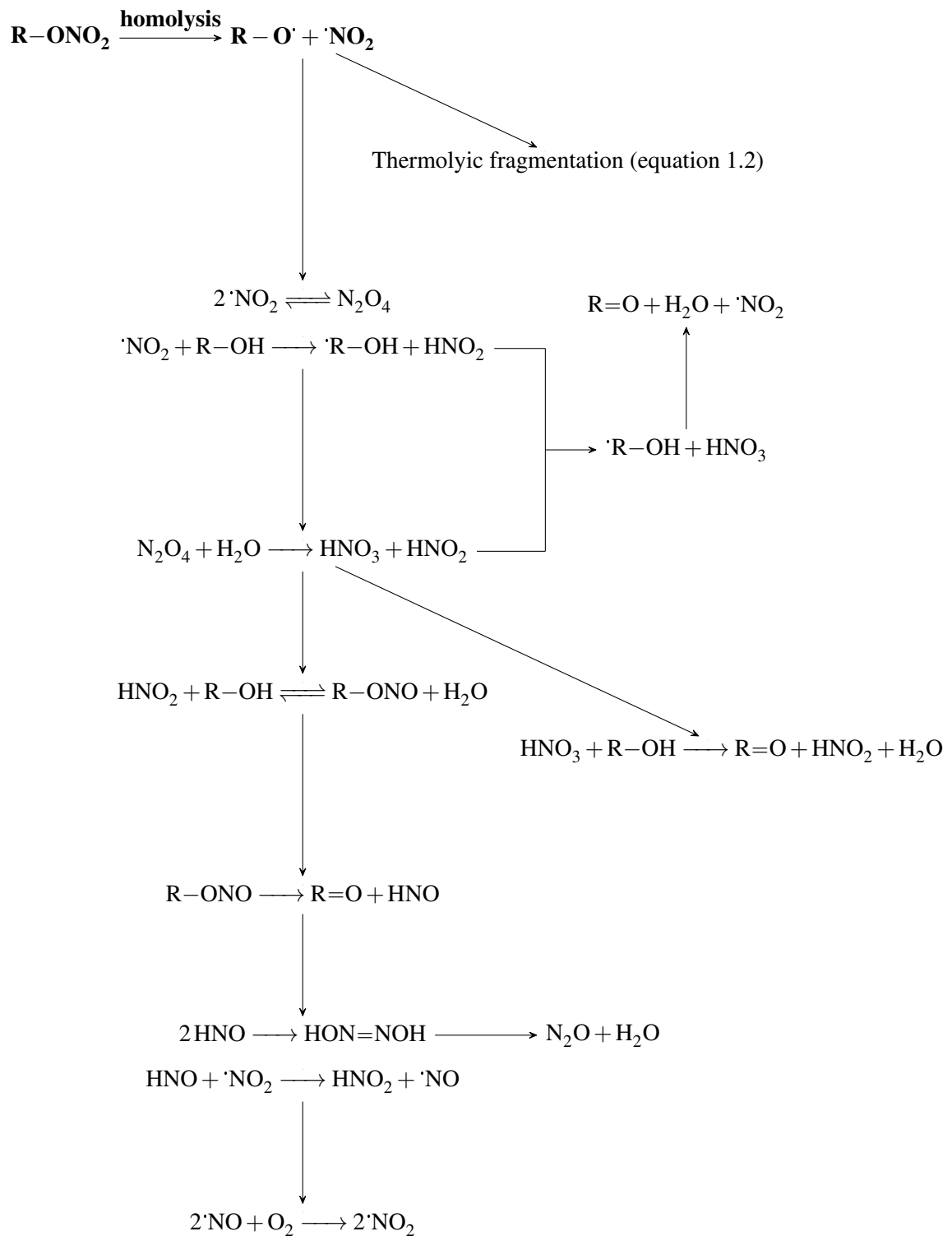
ergy of protonation, inspection of the reaction geometries shows that the bridging structure most resembles that expected for the liberation of the NO₂⁺ group at the next step. Though appearing less thermodynamically favourable when compared to protonation at the terminal upper oxygen site, the higher energy of reaction likely arises from the instability of the protonated complex. The elongation of the O-NO₂ bond allows stabilisation of the proton at the bridging site, facilitating the facile departure of NO₂⁺. Subsequent calculations involving the energy of the protonated EN will employ the values associated with the protonated bridging site.

Table 1.2 shows the energies for the reactions in all schemes, for both EN and the NC monomer.

The ωB97X-D long-range corrected hybrid functional (ωB97X-D) values obtained for the formation of N₂O₄ from 2'NO₂ are in good agreement with the experimentally recorded value of -1.4 kcal mol⁻¹ [20, 21]. It is noted that the Becke, 3-parameter, Lee-Yang-Parr hybrid functional (B3LYP) result does not perform so well for this reaction. This may arise from a number of factors, including the limitation to short-range interactions in B3LYP, or the geometry optimisation procedure, whereby a small variation or imperfect minimisation in the obtained optimised structures for the reaction species is amplified in the calculation of reaction energies. Comparison of reaction energies for EN and the monomer shows that most processes are more thermodynamically favourable in the case of NC.

1.4 Summary

A number of proposed reactions following the denitration of NC were validated by calculating energies of reaction with the ωB97X-D and B3LYP methods. It was found that except in the case nitric acid decomposition, 4HNO₃ ⇌ 4NO₂ + 2H₂O + O₂, most reactions were feasible at atmospheric conditions. The reactions were used to create rough schemes of the possible routes degradation routes, with increasing number of the NC decay. It can be seen

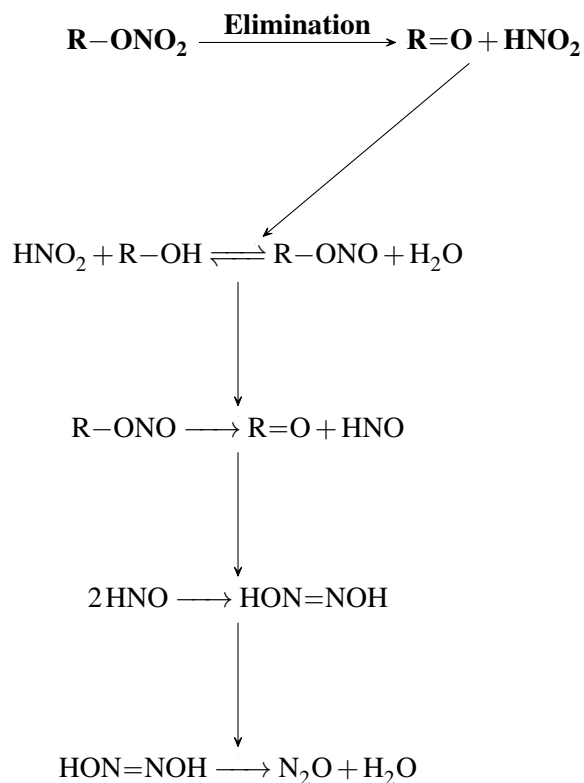


Scheme 1.5: Proposed degradation pathway starting from the homolytic fission of the nitrate ester, derived from the schemes presented by Camera [6] and Aellig[8].

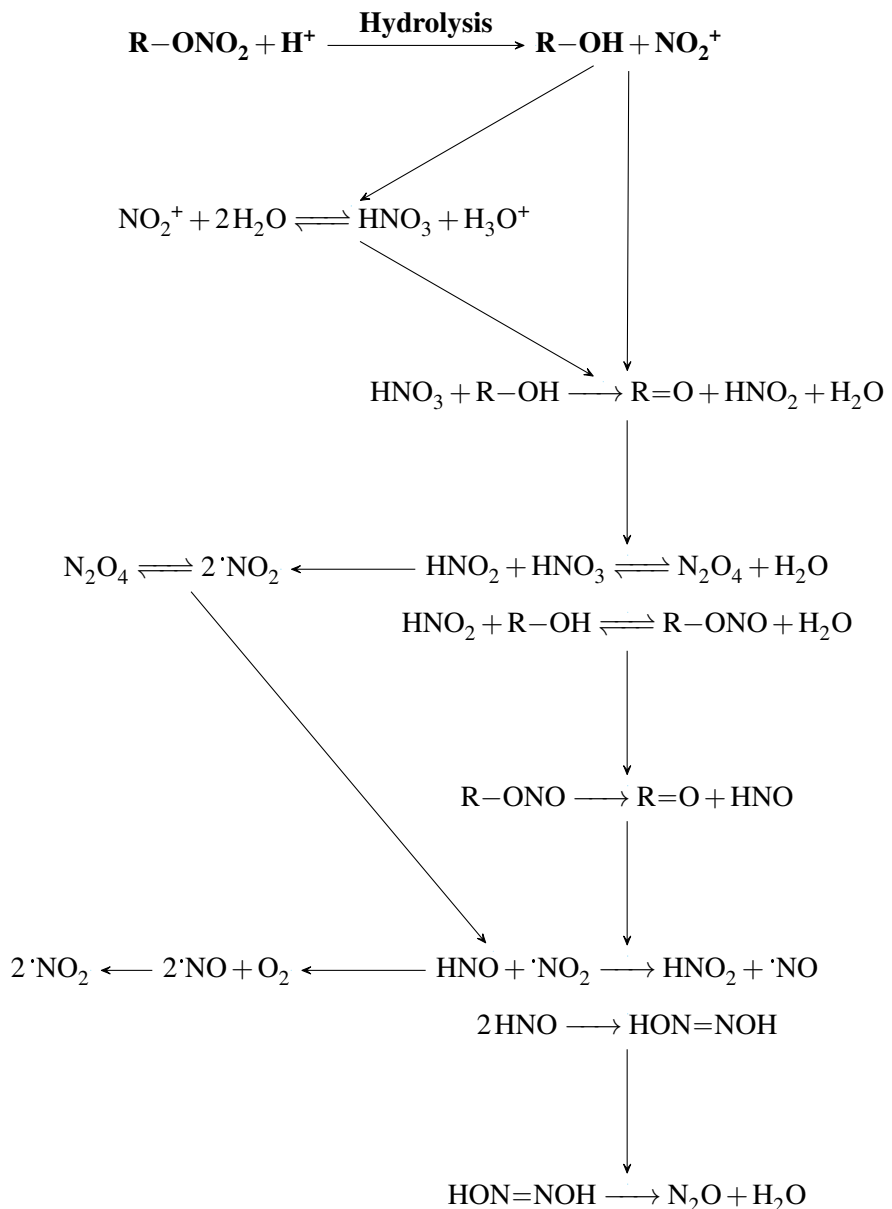
Table 1.2: Energies of nitrate ester decomposition reactions proposed by Camera [6], Chin [5] and Aellig [8]. R = CH₃CH₂ for EN, and R = (H₃CO)₂C₆H₉O₃ (bi-methoxy capped glutopyraonse monomer unit).

Reaction	$\Delta G_r / \text{kcal mol}^{-1}$			
	$\omega\text{B97X-D}$	PCM	B3LYP	PCM
N ₂ O ₄ + H ₂ O \longrightarrow HNO ₃ + HNO ₂	2.25	1.85	5.13	4.18
N ₂ O ₄ \rightleftharpoons 2·NO ₂	0.12	1.46	-0.54	-0.16
Radical reactions				
·NO ₂ + HNO \longrightarrow HNO ₂ + ·NO	-28.22	-28.67	-27.33	-27.63
2·NO + O ₂ \longrightarrow 2·NO ₂	-20.77	-21.97	-21.16	-22.16
Acid reactions				
HNO ₃ + HNO ₂ \rightleftharpoons N ₂ O ₄ + H ₂ O	-2.25	-1.85	-5.13	-4.18
4HNO ₃ \rightleftharpoons 4·NO ₂ + 2H ₂ O + O ₂	53.35	58.36	42.61	46.94
2HNO \longrightarrow HON=NOH	-38.97	-39.72	-36.63	-37.41
HON=NOH \longrightarrow N ₂ O + H ₂ O	-48.08	-48.18	-50.55	-50.75
Ionic reactions				
NO ₂ ⁺ + 2H ₂ O \rightleftharpoons HNO ₃ + H ₃ O ⁺	-0.90	-1.34	1.77	2.46
EN (R = CH ₃ CH ₂)				
R-ONO ₂ + H ₂ O \longrightarrow R-OH + HNO ₃	4.56	5.24	4.00	4.86
R-OH + HNO ₃ \longrightarrow R=O + HNO ₂ + H ₂ O	-34.06	-38.43	-37.59	-41.77
R-OH + ·NO ₂ \longrightarrow ·R-OH + HNO ₂	16.38	13.92	15.89	13.70
·R-OH + HNO ₃ \longrightarrow R=O + H ₂ O + ·NO ₂	-50.44	-52.35	-53.48	-55.47
R-OH + HNO ₂ \rightleftharpoons R-ONO + H ₂ O	-3.21	-3.28	-2.64	-2.95
R-ONO \longrightarrow R=O + HNO	-1.50	-5.82	-4.37	-8.50
NC monomer (R = (H ₃ CO) ₂ C ₆ H ₉ O ₃)				
R-ONO ₂ + H ₂ O \longrightarrow R-OH + HNO ₃	0.68	5.63	0.61	-0.70
R-OH + HNO ₃ \longrightarrow R=O + HNO ₂ + H ₂ O	-36.73	-38.34	-41.71	-41.70
R-OH + ·NO ₂ \longrightarrow ·R-OH + HNO ₂	14.71	11.15	13.03	23.21
·R-OH + HNO ₃ \longrightarrow R=O + H ₂ O + ·NO ₂	-51.44	-49.49	-54.75	-56.37
R-OH + HNO ₂ \rightleftharpoons R-ONO + H ₂ O	-4.43	-7.30	-4.31	-0.18
R-ONO \longrightarrow R=O + HNO	-2.93	-1.71	-6.82	-11.21

that it is the NO₂ species driving oxidation in all three schemes, and plays a central role in the extended degradation scheme of NC.



Scheme 1.6: Proposed degradation pathway starting from the elimination of HNO_2 from a nitrate ester, derived from the schemes presented by Camera [6] and Aellig[8].



Scheme 1.7: Proposed degradation pathway starting from the acid hydrolysis of a nitrate ester, derived from the schemes presented by Camera [6] and Aellig[8].

Bibliography

- [1] K. S. Hu, A. I. Darer, and M. J. Elrod. Thermodynamics and kinetics of the hydrolysis of atmospherically relevant organonitrates and organosulfates. *Atmospheric Chemistry and Physics*, 11(16):8307–8320, aug 2011.
- [2] M. Moniruzzaman and J.M. Bellerby. Use of UV visible spectroscopy to monitor nitrocellulose degradation in thin films. *Polymer Degradation and Stability*, 93(6):1067–1072, jun 2008.
- [3] Mohammed Moniruzzaman, John M. Bellerby, and Manfred A. Bohn. Activation energies for the decomposition of nitrate ester groups at the anhydroglucopyranose ring positions C2, C3 and C6 of nitrocellulose using the nitration of a dye as probe. *Polymer Degradation and Stability*, 102:49–58, apr 2014.
- [4] T. Sheppard, R. Behrens, D. Anex, D. Miller, and K. Anderson. Degradation chemistry of PETN and its homologues. Technical report, Sandia National Laboratories (SNL), Albuquerque, NM, and Livermore, CA (United States), nov 1997.
- [5] Anton Chin, Daniel S. Ellison, Sara K. Poehlein, and Myong K. Ahn. Investigation of the Decomposition Mechanism and Thermal Stability of Nitrocellulose/Nitroglycerine Based Propellants by Electron Spin Resonance. *Propellants, Explosives, Pyrotechnics*, 32(2):117–126, apr 2007.
- [6] E. Camera, G. Modena, and B. Zotti. On the Behaviour of Nitrate Esters in Acid Solution. II. Hydrolysis and oxidation of nitroglycerol and nitroglycerin. *Propellants, Explosives, Pyrotechnics*, 7(3):66–69, jun 1982.
- [7] Fotis Rigas, Ioannis Sebos, and Danae Doulia. Safety Charts Simulation of Nitroglycerine/Nitroglycerol Spent Acids via Chemical Reaction Kinetics. *Industrial and Engineering Chemistry Research*, 36(12):5068–5073, 1997.

- [8] Christof Aellig, Christophe Girard, and Ive Hermans. Aerobe Alkoholoxidation mithilfe von HNO₃. *Angewandte Chemie*, 123(51):12563–12568, dec 2011.
- [9] S. J. Buelow, D. Allen, G. K. Anderson, F. L. Archuleta, and J. H. Atencio. Destruction of Energetic Materials in Supercritical Water. Technical report, AIR FORCE RESEARCH LABORATORY, 2002.
- [10] L. Dauerman and Y. A. Tajima. Thermal decomposition and combustion of nitrocellulose. *AIAA Journal*, 6(8):1468–1473, aug 1968.
- [11] John W. Baker and D. M. Easty. Hydrolytic decomposition of esters of nitric acid. Part I. General experimental techniques. Alkaline hydrolysis and neutral solvolysis of methyl, ethyl, isopropyl, and tert.-butyl nitrates in aqueous alcohol. *Journal of the Chemical Society (Resumed)*, 1952(0):1193–1207, 1952.
- [12] E. Camera, G. Modena, and B. Zotti. On the behaviour of nitrate esters in acid solution. III. Oxidation of ethanol by nitric acid in sulphuric acid. *Propellants, Explosives, Pyrotechnics*, 8(3):70–73, jun 1983.
- [13] V. G. Matveev and G. M. Nazin. Stepwise Degradation of Polyfunctional Compounds. *Kinetics and Catalysis*, 44(6):735–739, nov 2003.
- [14] Juan F. Arenas, Francisco J. Avila, Juan C. Otero, Daniel Peláez, Juan Soto, and Juan Soto. Approach to the atmospheric chemistry of methyl nitrate and methylperoxy nitrite. Chemical mechanisms of their formation and decomposition reactions in the gas phase. *Journal of Physical Chemistry A*, 112(2):249–255, 2007.
- [15] Frank E. Wolf. Alkaline Hydrolysis Conversion of Nitrocellulose Fines. Technical Report October, Badger Army Ammunition Plant, oct 1997.
- [16] Russell D. Johnson III. NIST Computational Chemistry Comparison and Benchmark Database NIST Standard Reference Database Number 101, 2018.
- [17] I. Rodger and J. D. McIrvine. The decomposition of spent PETN nitration acids. *The Canadian Journal of Chemical Engineering*, 41(2):87–90, apr 1963.
- [18] Torbjörn Lindblom. Reactions in stabilizer and between stabilizer and nitrocellulose in propellants. *Propellants, Explosives, Pyrotechnics*, 27(4):197–208, sep 2002.

- [19] Hermann N. Volltrauer and Arthur Fontijn. Low-temperature pyrolysis studies by chemiluminescence techniques real-time nitrocellulose and PBX 9404 decomposition. *Combustion and Flame*, 41(C):313–324, jan 1981.
- [20] Neha Awasthi, Thomas Ritschel, Reinhard Lipowsky, and Volker Knecht. Standard Gibbs energies of formation and equilibrium constants from ab-initio calculations: Covalent dimerization of NO₂ and synthesis of NH₃. *Journal of Chemical Thermodynamics*, 62:211–221, jul 2013.
- [21] H. K. Roscoe and A. K. Hind. The equilibrium constant of NO₂ with N₂O₄ and the temperature dependence of the visible spectrum of NO₂: A critical review and the implications for measurements of NO₂ in the polar stratosphere. *Journal of Atmospheric Chemistry*, 16(3):257–276, apr 1993.